Alginate-Mediated Growth of Co, Ni, and CoNi Nanoparticles: Influence of the Biopolymer Structure

Roberta Brayner,*,§ Marie-Josèphe Vaulay,§ Fernand Fiévet,§ and Thibaud Coradin*,†

Interfaces, Traitements, Organisation et Dynamique des Systèmes (ITODYS), CNRS-UMR 7086, Université Denis Diderot, 2 place Jussieu, 75251 Paris Cedex 05, France, and Chimie de la Matière Condensée de Paris (CMCP), CNRS-UMR 7574, Université Pierre et Marie Curie, 4 Place Jussieu, 75252 Paris Cedex, France

Received October 30, 2006. Revised Manuscript Received December 14, 2006

Biopolymers have already been widely used to control the growth of inorganic particles. However, some of these natural macromolecules present an intrinsic chemical and structural variability that may influence their templating efficiency. We have therefore compared the ability of three different sources of alginate to control the formation of Co, Ni, and CoNi nanoparticles. Variations in particle size, structure, and magnetic properties were observed depending on the alginate composition. The more stable gels allowed the formation of Co_xNi_{100-x} nanoalloys over the whole solid solution domain. Moreover, these networks stabilize Ni nanoparticles in an unusual hexagonal compact phase. These results could be related to the strength of the metal−alginate gels and hence to the metal ion coordination within the polymer network. They also point out some possible limitations in the use of natural polymers for biocomposite design.

Introduction

The use of polymer networks as controlled environments for the synthesis of metal nanoparticles has been widely studied.[1] These approaches allow a precise control of the nanoparticle size, shape, and three-dimensional organization.[2,3] In this context, recent concerns for eco-friendly "green" processes triggered many studies devoted to the suitability of biopolymer gels to achieve such a controlled growth of metallic nanoparticles.[4−8]

So far, one of the most studied biological macromolecule for such approaches is alginic acid (alginate) due to several interesting features : (i) it is extracted from a brown marine algae (*Phaeophyceae*) widely found over the planet's coasts; (ii) it presents a very particular process leading to gel formation. Alginic acid or alginate is the common term applied to a family of linear polysaccharides containing 1,4-linked β-D-mannuronic (M) and α-L-guluronic (G) acid residues arranged in a block-wise, nonregular order along the chain.[9] The proportion of M and G residues and their macromolecular conformation determine the physical properties and the affinity of the alginate for divalent metals.[10,11] Alginates are able to adopt an ordered conformation through dimerization of the poly-G sequences in the presence of Ca^{2+} or other divalent cations, and this description is known as the "egg-box" model.[12] Dimerization regions are terminated by chain sequences of poly-M or mixed poly-MG, and several different chains may become interconnected promoting gel network formation. Alginate gels have already been used to control the growth of Au, Ag, Co, and Ni nanoparticles as well as Te nanowires.[13−16]

One particular problem when using macromolecules from biological origin, and more specifically polysaccharides, is that the precise composition and structure of the polymer backbone can significantly depend on the living organisms it is extracted from. Such variations may, in turn, modify the properties of the resulting gels.[17] For instance, it was shown, in the case of alginate, that the M/G ratio has a great influence on their biocompatibility.[18]

To address this problem, we have studied three different types of alginate and evaluate their suitability to control the growth of Co and Ni nanoparticles as well as CoNi

* Corresponding authors. E-mail: brayner@ccr.jussieu.fr (R.B.) and coradin@ccr.jussieu.fr (T.C.).
§ ITODYS.
† CMCP.

(1) Caseri, W. *Macromol. Rapid Commun.* **2000**, *21*, 705.
(2) Zhang, J.; Xu, S.; Kumacheva, E. *J. Am. Chem. Soc.* **2004**, *126*, 7908.
(3) Shenhar, R.; Norsten, T. B.; Rotello, V. M. *Adv. Mater.* **2005**, *17*, 657.
(4) Raveendran, P.; Fu, J.; Wallen, S. L. *J. Am. Chem. Soc.* **2003**, *125*, 13940.
(5) He, J.; Kunitake, T.; Nakao, A. *Chem. Mater.* **2003**, *15*, 4401.
(6) Sarma, T. K.; Chattopadhyay, A. *Langmuir* **2004**, *20*, 3520.
(7) Singh, A. V.; Bandgar, B. M.; Kasture, M.; Prasad, B. L. V.; Sastry, M. *J. Mater. Chem.* **2005**, *15*, 5115.
(8) Brayner, R.; Coradin, T.; Vaulay, M. J.; Mangeney, C.; Livage, J.; Fiévet, F. *Colloids Surf. A.* **2005**, *256*, 191.
(9) Chanda, S. K.; Hirst, E. L.; Percival, B. G. V.; Ross, A. G. *J. Am. Chem. Soc.* **1952**, 1833.
(10) (a) Smidsrod, O.; Haug, A. *Acta Chem. Scand.* **1965**, *19*, 329. (b) Smidsrod, O.; Haug, A. *Acta Chem. Scand.* **1965**, *19*, 341.
(11) Zheng, H. *Carbohydr. Res.* **1997**, *302*, 97.
(12) (a) Grant, G. T.; Morris, E. R.; Rees,, D. A.; Smith, P. J. C.; Thom, D. *FEBS Lett.* **1973**, *32*, 195. (b) Morris, E. R.; Rees, D. A.; Thom, D.; Boyd, J. *Carbohydr. Res.* **1978**, *66*, 145.
(13) Torres, E.; Mata, Y. N.; Blazquez, M. L.; Munoz, J. A.; Gonzalez, F.; Ballester, A. *Langmuir* **2005**, *21*, 7951.
(14) Pal, A.; Esumi, K.; Pal, T. *J. Colloid Interface Sci.* **2005**, *288*, 396.
(15) Brayner, R.; Coradin, T.; Fiévet-Vincent, F.; Livage, J.; Fiévet, F. *New J. Chem.* **2005**, *29*, 681.
(16) Lu, Q.; Gao, F.; Komarneni, S. *Adv. Mater.* **2004**, *16*, 1629.
(17) Barbotin, J. N.; Nava Saucedo, J. E. in *Poly-saccharides: Structural Diversity and Functionnal Versatility*; Dimitriu, S., Ed; Marcel Dekker: New York, 1996; p 125.
(18) Orive, G.; Hernandez, P. R. M.; Gascon, A. R.; Igartua, M.; Pedraz, J. L. *Biomaterials* **2002**, *23*, 3825.

10.1021/cm062580q CCC: $37.00
Published on Web 02/06/2007

nanoalloys under reducing conditions. The M/G ratio is revealed to strongly influence the structure of resulting metallic nanoparticles. In particular, a low M/G ratio favors the unusual formation of the hexagonal compact phase of Ni. In addition, Co_xNi_{100-x} nanoalloys could be obtained over the whole domain of composition ($0 \leq x \leq 100$). These results enlighten the role of the metal ion sequestration in the alginate microgel domains on the control of the nanoparticle growth. They also demonstrate that the intrinsic chemical and structural variability of some bio-macromolecules should be taken into account when these polymers are used as templating agents for the controlled formation of inorganic materials.

Experimental Section

Three commercial sources of alginate were used: alginic acid sodium salt from brown algae from Fluka (Alg-1), alginic acid sodium salt from Aldrich (Alg-2), and alginic acid sodium salt from *Macrocystis pyrifera*, low viscosity from Sigma (Alg-3). From the suppliers, Alg-1 is of type G (low M/G ratio), Alg-3 is of type M (high M/G ratio), and finally Alg-2 has an intermediate M/G ratio. Ni^{2+} and Co^{2+} chlorides were purchased from Sigma.

Ni^{2+}, Co^{2+}, and mixed $Ni^{2+}Co^{2+}$−alginate microcapsules were obtained from 1.5 wt % alginate polymer solutions dropped into 0.1 M aqueous solution of $NiCl_2$, $CoCl_2$, or both salts under mild stirring. Droplets of the alginate solution were extruded through a needle tip and fall into the aqueous solution containing divalent cations. Gelation immediately occurs at the droplet surface to form spherical capsules, which are further cross-linked by slow cation diffusion toward the core of the beads. After 1 h, the microcapsules were recovered by filtration and thoroughly washed with demineralized water until a clear solution was obtained. To avoid metal agglomeration (due to the presence of water inside the microcapsules) during reduction reaction, all samples were freeze-dried at −80 °C using a ALPHA 2-4 apparatus. Finally, the microcapsules were reduced under flowing H_2/N_2 in a tubular oven at 350 °C for 4 h.

Fourier transform infrared (FT-IR) experiments were performed in transmission mode using a Equinox 55 Brucker FT-IR spectrometer. The spectra were averaged over 200 scans at a resolution of 4 cm^{-1} between 4000 and 400 cm^{-1}.UV−visible−near-infrared diffuse reflectance spectra were recorded on a Cary 5E spectrophotometer equipped with a poly(tetrafluoroethylene)-coated integration sphere. Differential thermal analysis−thermogravimetric analysis measurements were performed on a SETARAM thermobalance. X-ray powder diffraction (XRD) patterns were recorded using a Cu Kα radiation. The diffractometer was calibrated using a standard Si sample. The counting time was 30 s per step of 0.05° 2θ. The mean crystallite size was estimated using the Scherrer equation.

X-ray energy dispersive spectrometry (EDX) was performed using a (EDXD) EDAX system equipped with a super ultrathin window connected to a JEOL JSM 6100 scanning electron microscope operating at 25 kV. Atomic compositions (%) were obtained with Genesis software. Transmission electron microscopy (TEM) measurements were performed with a JEOL 100CXII operating at 100 kV. Mean particle diameters were estimated from image analysis using a digital camera and the SAISAM and TAMIS softwares (Microvision Instruments).

Magnetic measurements were performed using a Quantum Design MPMS-5S SQUID magnetometer in the temperature range 2−300 K.

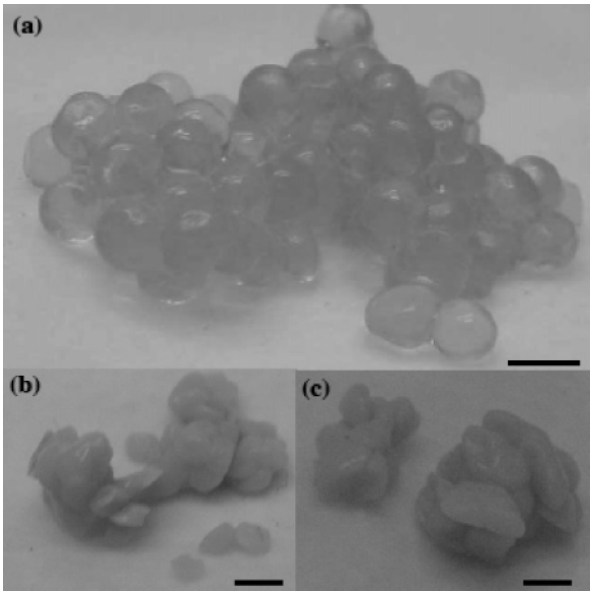

Figure 1. Alginate beads morphology in the presence of Co^{2+} for (a) Alg-1, (b) Alg-2, and (c) Alg-3 (scale bar = 2 mm).

Results and Discussion

Microcapsule Formation and Spectroscopic Studies. Three series of alginate (Alg-1, Alg-2, and Alg-3) with different Co^{2+}/Ni^{2+} ratios were prepared using 1.5 wt % of alginate and 0.1 M cation concentration corresponding to the conditions most frequently found in the literature and considered as optimal for capsule synthesis.[19]

After being filtered and rinsed, Alg-1 series present transparent pink (Co^{2+}) and green (Ni^{2+}) microcapsules with homogeneous spherical shape and diameters in the 1.0−2.0 mm range (Figure 1a). Alg-2 and Alg-3 series present opaque pink (Co^{2+}) and green (Ni^{2+}) microcapsules diameters similar to Alg-1 samples but with heterogeneous shape (Figure 1b,c). Studies by optical microscopy also reveal that, for Alg-1 series, size and morphology of these microcapsules depend on the Co^{2+}/Ni^{2+} ratio (Figure 2). Alg-1 Co presents high deformation (Figure 2a) while Alg-1 Ni shows a perfect sphere (Figure 2e), and the sphericity evolution was observed for intermediate Co^{2+}/Ni^{2+} ratios. The deformation of alginate beads was shown to be related to the strength of the gel network.[19] Thus, these data indicate that the stability of the beads decreases when M/G ratio increases and that Co^{2+} leads to less stable gels than Ni^{2+}.

The composition of hybrid microcapsules was quantified by EDX measurements (Table 1). For Co−alginate and Ni−alginate beads, the carbon-to-metal ratios are similar for a given polymer and increase with the M/G ratio, indicating that the amount of adsorbed cations is directly linked to the presence of guluronate groups. For CoNi capsules, the cobalt-to-nickel ratio is very close to the initial content of the solutions, but with a systematic excess of Ni ions. Such a result is in agreement with reported data on the activation energy E_a of metal−alginate complex formation, indicating a slightly lower value for Ni^{2+} (122 kJ mol^{-1}) when compared to Co^{2+} (142 kJ mol^{-1}).[20]

(19) Nava Saucedo, J. E.; Audras, B.; Jan, S.; Bazinet, C. E.; Barbotin, J. N. *FEMS Microbiol. Rev.* **1994**, *14*, 93.

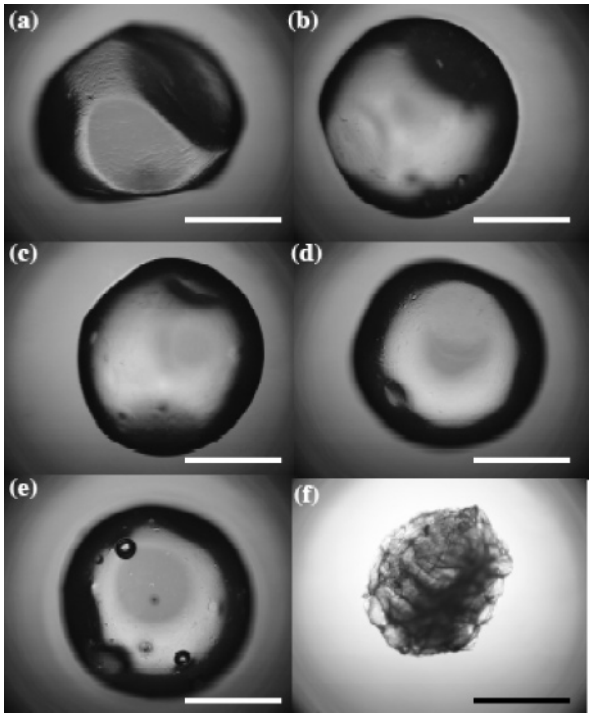

Figure 2. Optical microscopy images of wet (a) Alg-1 Co, (b) Alg-1 75Co25Ni, (c) Algi-1 50Co50Ni, (d) Alg-1 25Co75Ni, and (e) Alg-1 Ni and freeze-dried Alg-1 Co (scale bar = 0.5 nm).

Table 1. C, Co, and Ni Concentrations (in atom %) Obtained by EDX Analysis

sample	C (atom %)/ M[a] (atom %)	Co (atom %)/ Ni (atom %)
Alg-1 Ni	1.18	
Alg-1 25Co75Ni		0.28
Alg-1 50Co50Ni		0.79
Alg-1 75Co25Ni		2.76
Alg-1 Co	1.05	
Alg-2 Ni	2.05	
Alg-2 25Co75Ni		0.27
Alg-2 50Co50Ni		0.74
Alg-2 75Co25Ni		2.55
Alg-3 Ni	2.75	
Alg-3 25Co75Ni		0.30
Alg-3 50Co50Ni		0.89
Alg-3 75Co25Ni		2.65

[a] M = Co, Ni.

As previously reported, the FT-IR spectra of alginates containing different M/G ratios show some variations in relative band intensities.[21,22] Figure 3 presents FT-IR spectra of the three series of alginate with Ni^{2+}, and Table 2 indicates peak attribution according to Sartori et al.[22] Figure 3b shows a fingerprint region from Figure 3a. For Alg-1, the bands or shoulders around 1420, 1330, 1130, 1090, 1020, 1000, and 950 cm^{-1} are of greater intensity than for Alg-2 and Alg-3. On the other hand, the bands or shoulders at 1440, 1300, 880, and 820 cm^{-1}, are most pronounced for Alg-3, and in all cases, Alg-2 presents intermediary intensities close to Alg-1. The first set of wavenumbers is characteristic of guluronic acid (G) while the second set is typical of mannuronic acid

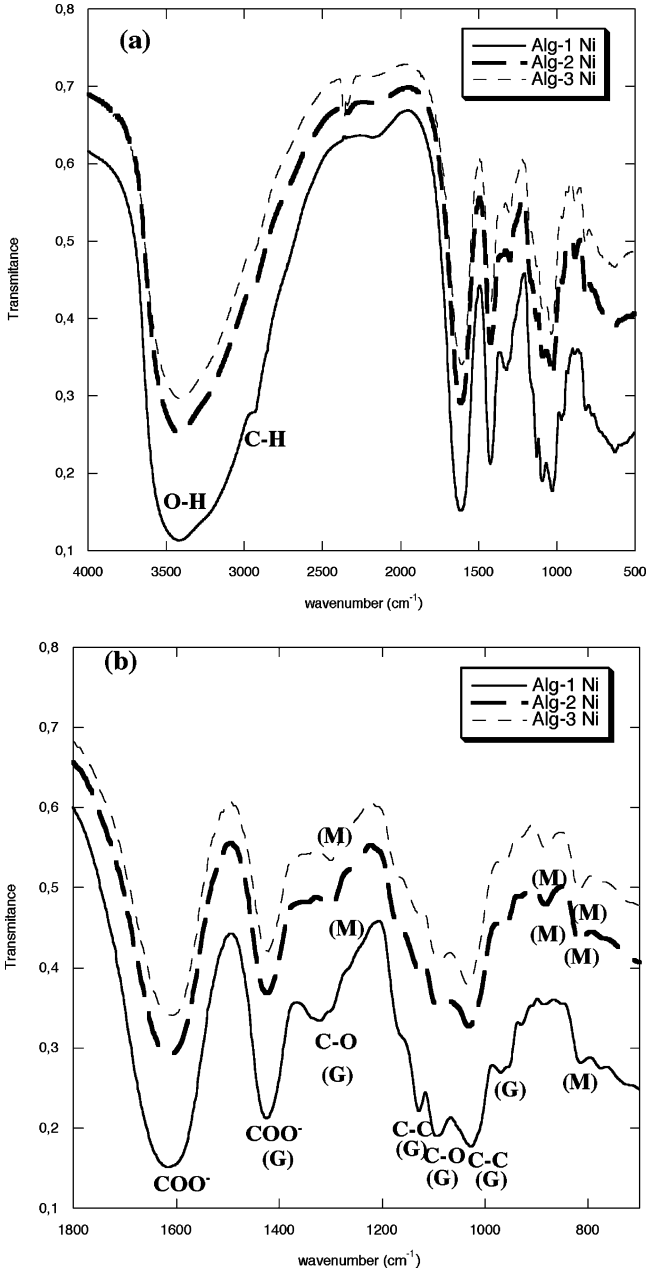

Figure 3. (a) FT-IR spectra of three different lyophilized alginate−Ni and (b) fingerprint region (between 1800 and 700 cm^{-1}).

(M).[22] These results confirm that Alg-1 is of type G (low M/G ratio), and Alg-3 is of type M (high M/G ratio).

The environment of the cations within the alginate framework was studied using UV−visible spectroscopy (Figure 4). The corresponding absorption wavelengths and assignments of the observed bands are given in Table 3. In a previous work, we characterized Co^{2+} and Ni^{2+} alginates before freeze-drying, and in this case, all alginate microcapsules presented Co^{2+} and Ni^{2+} exclusively in the octahedral coordination in a weak ligand field.[15] Here, hybrid alginates were also analyzed after freeze-drying. For Co^{2+} sample, a color modification was observed from pink to blue due to a coordination change from octahedral to tetrahedral. It is well-known that cobalt hydroxide can be crystallized into a hexagonal layered structure with two polymorphs: α and β.[23−26] β-$Co(OH)_2$ possesses a brucite-like origin, where octahedra with divalent cobalt cations 6-fold coordinated by

(20) Hassan, R. M.; Makhlouf, M. T.; El-Shatoury, S. A. *Colloid Polym. Sci.* **1992**, *270*, 1237.
(21) Mackie, W. *Carbohydr. Res.* **1971**, *20*, 413.
(22) Sartori, C.; Finch, D. S.; Ralph, B.; Gilding, K. *Polymer* **1997**, *38*, 43.

Table 2. FT-IR Band Assignments for Different Lyophilized Alginate−Ni Samples

wavenumber (cm^{-1})	intensity[a]	assignment[b]
3360−3380	v.s.	O−H stretch.
3250	s.	O−H stretch.
2930−2932	w.	C−H stretch.
2750	w.	C−H stretch.
1608−1611	v.s.	COO^- stretch.
1413−1420	m.	COO^- stretch.
1317	w.	C−O stretch.
1294	w.	C−O stretch.
1176	w.	C−O stretch.
		C−C stretch.
		C−C−C bend.
1124−1130	m.	C−C stretch.
		C−O stretch.
1087−1090	m.	C−O stretch.
		C−O−C stretch.
1020	m.	O−H bend.
947−950	w.	C−O stretch.
		C−C−H stretch.
880	w.	C−C stretch.
		C−C−H bend.
		C−O bend.
781−820	w.	C−O intern. rot.
		C−C−O bend.
		C−C−H bend.

[a] Abbreviations: v.s. = very strong, s. = strong, m.= medium, w. = weak. [b] Abbreviations: stretch = stretching, bend. = bending, intern. rot. = internal rotation.

hydroxyl ions share edges to produce two-dimensional charge-neutral layers stacked one over the other along the *c* direction without any intercalated species.[23,25] The β phase exhibits a characteristic pink color. On the other hand, the α phase consists of positively charged layers with anions (CO_3^{2-}, NO_3^-, Cl^-, ...), and in this case, water molecules reside in the gallery to restore charge neutrality.[17,27,28] This causes an important expansion in the interlayer spacing, and the color also changes from pink to green/blue. The UV−visible measurements also support the occurrence of tetrahedral Co^{2+} coordination in the alginate matrix. Figure 4a shows the comparison of UV−visible diffuse reflectance spectra of alginate−Co^{2+} before and after freeze-drying. In the visible region, broad absorption bands centered at ∼465 and ∼520 nm were observed for α and β phases, respectively. In addition, strong peaks at ∼625 and ∼665 nm were observed only for the α phase. The spectroscopic features of α-type Co^{2+} in alginate matrix are in good agreement with the literature showing that tetrahedron-containing cobalt compounds typically exhibit peaks at lower energies due to the presence of Co^{2+} d−d absorption in tetrahedral coordination geometry.[29,30] The transition energies for the two peaks were calculated to be $\sim 1.5 \times 10^4$ and 1.6×10^4 cm^{-1}, in agreement with the reported values for tetrahedral coordination, $\nu_3(T_d) = 15596$ and 16883 cm^{-1}.[31] Moreover, Ni^{2+}, in

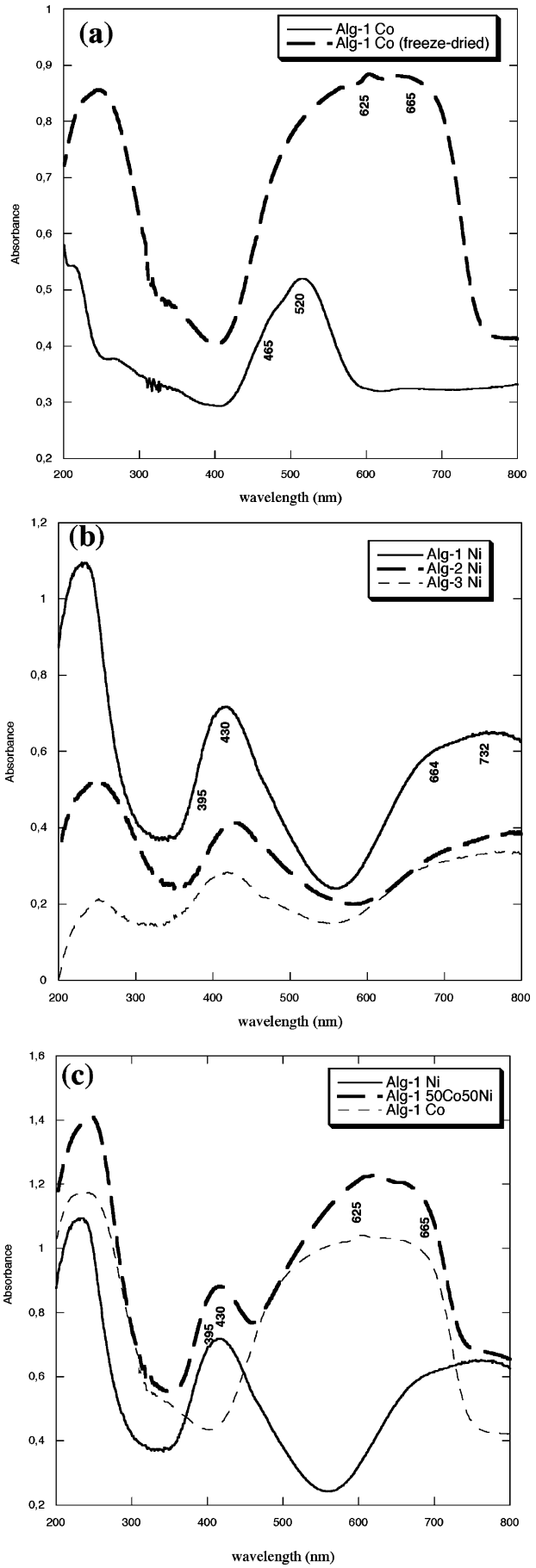

Figure 4. UV−visible spectra of (a) alginate−Ni^{2+}, (b) alginate−Co^{2+}, and (c) alginate−$Ni^{2+}Co^{2+}$ microcapsules.

(23) Benson, P.; Briggs, G. W. D.; Wynne-Jones, W. F. K. *Electrochim. Acta* **1964**, *9*, 275.
(24) Bish, D. L.; Livingstore, A. *Miner. Magn.* **1981**, *44*, 339.
(25) Mockenhaupt, Ch.; Zeiske, Th.; Lutz, H. D. *J. Mol. Struct.* **1998**, *443*, 19.
(26) Ma, R.; Liu, Z.; Takada, K.; Fukuda, K.; Ebina, Y.; Bando, Y.; Sasaki, T. *Inorg. Chem.* **2006**, *45*, 3964.
(27) Delahaye-Vidal, A.; Figlarz, M. *J. Appl. Electrochem* **1987**, *17*, 589.
(28) Rajamathi, M.; Subbanna, G. N.; Kamath, P. V. *J. Mater. Chem.* **1997**, *7*, 2293.
(29) Jayashree, R. S.; Kamath, P. V. *J. Mater. Chem.* **1999**, *9*, 961.
(30) Poul, L.; Juini, N.; Fiévet, F. *Chem. Mater.* **2000**, *12*, 3123.

Table 3. UV−Visible Absorption Wavelength and Band Assignment for Alginate Microcapsules

sample	wavelength (nm)	assignment
Alg−Ni^{2+}_{Oh}	985	ν_1: $^3T_{2g}(F) \leftarrow {}^3A_{2g}(F)$
	732	ν_2: $^3T_{1g}(F) \leftarrow {}^3A_{2g}(F)$
	664	$^1E_g \leftarrow {}^3A_{2g}(F)$
	430	$^1T_{1g} \leftarrow {}^3A_{2g}(F)$
	395	ν_3: $^3T_{1g}(P) \leftarrow {}^3A_{2g}(F)$
Alg−Co^{2+}_{Oh}	1211	ν_1: $^4T_{2g}(F) \leftarrow {}^4T_{1g}(F)$
	476, 516	ν_3: $^4T_{1g}(P) \leftarrow {}^4T_{1g}(F)$
Alg−Co^{2+}_{Td}	465, 625, 665	ν_3 : $^4T_1(F) \leftarrow {}^4A_2(F)$

the same conditions, remains exclusively in the octahedral coordination (Table 3, Figures 4b,c). For freeze-dried alginate−Ni^{2+} microcapsules, the calculated crystal field Δ_{Oh} (8230 cm^{-1}, average value obtained from Δ_{Oh} for ν_1 and ν_2) and Racah parameter B (973 cm^{-1}) are close to the β-Ni(OH)$_2$ values ($\Delta_{Oh} = 8600$ cm^{-1}; $B = 985$ cm^{-1}).[32,33] These data also confirm the previous assumption on the stronger bonding of Ni^{2+} when compared to Co^{2+}. Figure 4b shows UV−visible spectra of hybrid alginate−$Ni^{2+}Co^{2+}$ after freeze-drying corresponding to the sum of the contributions of octahedral Ni^{2+} and tetrahedral Co^{2+} coordination. Finally Figure 4c presents the comparison of UV−visible spectra of freeze-dried Alg-1 Ni, Alg-2 Ni, and Alg-3 Ni prepared from the same Ni^{2+} solution (0.1 M). In this case, the absorption bands intensity decreases when the M/G ratio increases, in agreement with EDX data.

Differential thermal analyses (DTA) of freeze-dried hybrid alginate−Ni^{2+} samples (Figure 5) were carried out under oxygen. For all samples, an exothermic peak was observed at 305 °C which corresponds to the formation of water and CO_2 through the dehydrogenation reaction and combustion of carboxylate anions (partial decomposition of the alginate matrix).[34] The intensity of this peak increases with the M/G ratio in agreement with the increase of the carbon-to-nickel ratio observed by EDX data. This combustion catalyzes the formation of nickel oxide (NiO). For Alg-1 Ni, NiO formation corresponds to a strong exothermic effect at 463 °C. For Alg-2 Ni and Alg-3 Ni, the exothermic effect is less important, probably due to the lowest amount of immobilized Ni^{2+}. Moreover, it occurs at lower temperatures, between 400 and 425 °C, once again because of the increased number of carboxylate groups per nickel ions.

Metallic Nanoparticle Formation and Structural Characterization. The reduction of hybrid polycation alginates at 350 °C, under flowing 10% H_2/N_2, leads to the formation of metallic nanoparticles in alginate matrix. It is important to note that, for all alginate based materials, no sintering was observed at up to 400 °C in reduction conditions due to the high-temperature resistance of the alginate network. Table 4 and Figure 6 shows nanoparticles mean diameter and their morphologies. Observed diameters vary between 10 and 25 nm. In most cases, crystallite sizes inferred from X-ray line broadening compared to particles sizes obtained from TEM are quite similar, indicating that each particle is a single crystal.

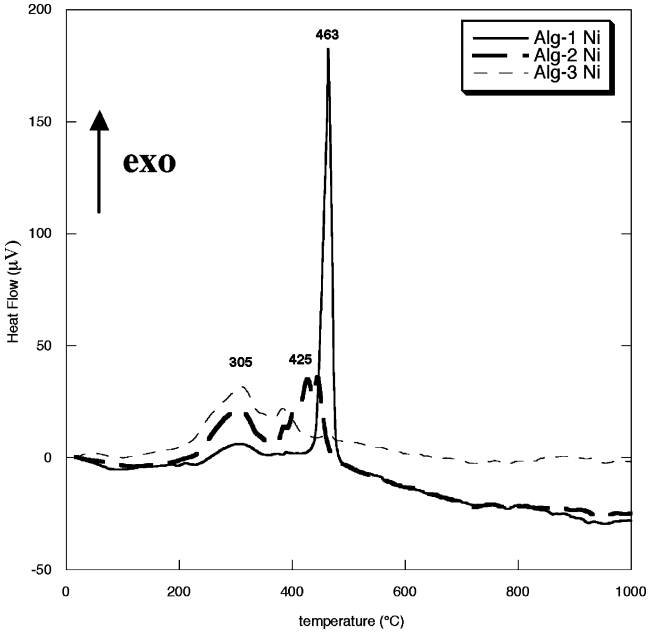

Figure 5. DTA measurements of hybrid alginate−Ni^{2+} samples.

Table 4. Mean Crystallite Size (from XRD, ϕ_m), Mean Diameter (from TEM, d_m), Standard Deviation (σ), and Relative Deviation (σ/d_m) of Metallic Nanoparticles inside Alginate Matrixes

sample	ϕ_m (nm)	d_m (nm)	σ (nm)	σ/d_m
Alg-1 Ni	20.0	25.2	0.89	0.04
Alg-1 25Co75Ni	22.4	35.3	4.80	0.14
Alg-1 50Co50Ni	15.9	19.7	2.12	0.11
Alg-1 75Co25Ni	16.3	26.0	2.63	0.10
Alg-1 Co	20.0	25.4	1.18	0.05
Alg-2 Ni	14.2	20.0	1.53	0.08
Alg-2 25Co75Ni	15.4	15.1	1.54	0.10
Alg-2 50Co50Ni	14.6	23.7	2.64	0.11
Alg-2 75Co25Ni	14.4	10.0	0.98	0.09
Alg-2 Co	29.6	20.0	4.95	0.25
Alg-3 Ni	10.0	15.3	2.02	0.13
Alg-3 25Co75Ni	20.1	13.2	1.50	0.11
Alg-3 50Co50Ni	24.3	22.1	2.05	0.09
Alg-3 75Co25Ni	24.8	22.2	2.58	0.12
Alg-3 Co	29.5	25.0	3.20	0.13

Co-alginate samples present only a hexagonal compact (hcp) phase (Figure 7a), as expected from the reported temperature of ca. 420 °C for the hcp-to-face centered cubic (fcc) phase for cobalt.[35] Alg-1 Co also shows the presence of cobalt oxide. This was confirmed by XPS measurements (not shown), indicating a CoO layer thickness of ca. 0.4 nm. Moreover, the mean crystallite size was similar for both [10.0] and [00.2] directions, which means that the crystallites are nearly isotropic. In addition, no widening of the (10.1) line was observed which means absence of stacking faults.[36] Monometallic Ni samples exhibit a very narrow particle size distribution in all alginate matrixes. Alg-1 Ni and Alg-2 Ni samples present mixed fcc and hcp structures (Figure 7b). Alg-1 Ni presents higher hcp phase percentage than Alg-2 Ni. Alg-3 Ni shows only fcc phase. Indeed, Ni powders usually crystallize with a fcc structure. The hcp phases can be obtained at low-temperature using organic templates but

(31) Stahlin, W.; Oswald, H. R. *Acta Crystallogr.* **1970**, *B26*, 860.
(32) Minkova, N.; Krusteva, M.; Nikolov, G. *J. Mol. Struct.* **1984**, *115*, 23.
(33) Dou, Y. S. *J. Chem. Educ.* **1990**, *67*, 134.
(34) Zohuriaan, M. J.; Shokrolahi, F. *Polym. Testing* **2004**, *23*, 575.
(35) Greenwood, N. N.; Earnshaw, A. *Chemistry of the Elements*, 2nd ed.; Elsevier: Oxford, 1997, p 1115.
(36) Warren, B.E. *X-ray diffraction*; Dover Publications: New York, 1990.

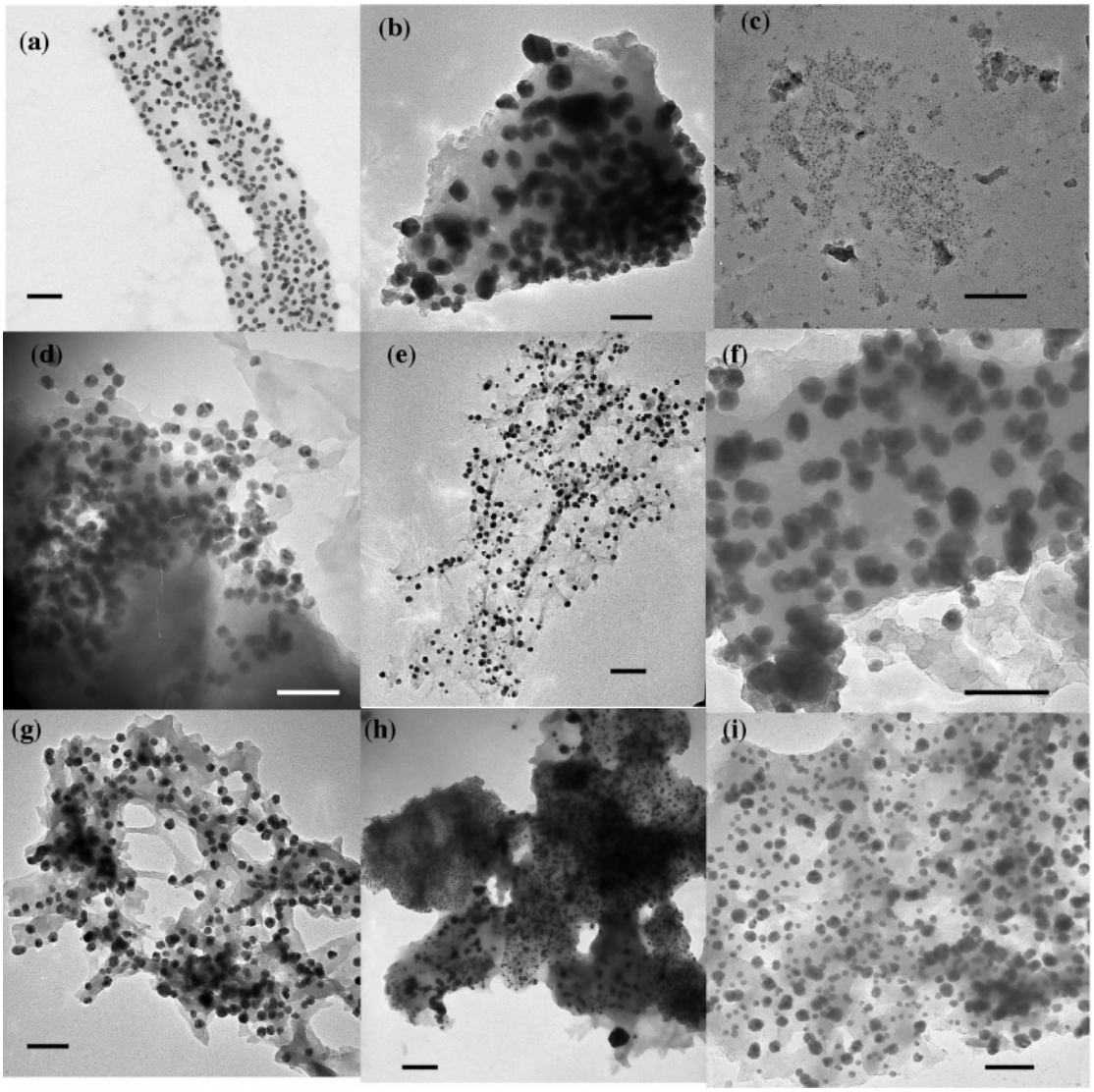

Figure 6. TEM micrographs of (a) Alg-1 Ni, (b) Alg-1 25Co75Ni, (c) Alg-1 Co, (d) Alg-2 Ni, (e) Alg-2 25Co75Ni, (f) Alg-2 Co, (g) Alg-3 Ni, (h) Alg-3 25Co75Ni, and (i) Alg-3 Co (scale bar = 100 nm).

are easily converted to fcc upon heating.[37,38] Another possibility to stabilize hcp is to use epitaxial approaches.[39] In our case, the stabilization of hcp appears favored by the alginate network, and this process is all the more efficient as the initial gel is cross-linked. This suggests that the "egg-box" cavity intrinsic anisotropy may favor the growth of anisotropic hcp platelets.

The addition of Ni to Co to form NiCo alloys was expected to favor the formation of fcc phase. In fact, for the mixed NiCo−alginate samples, after reduction at 350 °C, a solid solution is obtained (Figure 7c,d). Furthermore, the accurate determination of the lattice parameters of the Alg-1 NiCo fcc phase shows a linear dependence against composition over the entire metal composition rage (Figure 8a). Such a linear dependence, which agrees with Vegard's law, has been previously reported for bulk alloys and for CoNi particles prepared by the "polyol" process.[40,41] Unfortunately, it was not possible to determine with precision the lattice parameters of Alg-2 NiCo and Alg-3-NiCo (not shown) because the XRD background was very high, due to the important amount of residual carbon. This ability of alginate to allow such nanoalloys suggests that Co^{2+} and Ni^{2+} ions are located in close vicinity to each other, probably within the egg-box cavities of the gel.

Nanoparticle Magnetic Properties. Table 5 summarizes the principal magnetic properties of alginate-based NiCo microcapsules as inferred from superconducting quantum interference device (SQUID) at 2 K. For monometallic Co samples, the saturation magnetization (M_s) values at 5 T are slightly lower than the bulk value (160 emu g^{-1}). This can be attributed to the presence of the passivating surface layer of cobalt oxide. On the other hand, for monometallic Ni samples, the M_s values are not far from the bulk value (63 emu g^{-1}). All bimetallic NiCo samples present M_s values much lower than the value for the bulk $Co_{80}Ni_{20}$ alloy (138

(37) Hinotsu, T.; Jeyadevan, B.; Chinnasamy, C. N.; Shinoda, K.; Tohji, K. *J. Appl. Phys.* **2004**, *95*, 7477.
(38) Jeon, Y. T.; Moon, J. Y.; Lee, G. H.; Park, J.; Chang, Y. *J. Phys. Chem.* **2006**, *110*, 1187.
(39) Tian, W.; Sun, H. P.; Pan, X. Q.; Yu, J. H.; Yeadon, M.; Boothroyd, C. B.; Feng, Y. P.; Lukaszew, R. A.; Clarke, R. *Appl. Phys. Lett.* **2005**, *86*, 131915.
(40) Taylor, A. J. *Inst. Metals* **1950**, *77*, 585.
(41) Toneguzzo, Ph.; Viau, G.; Acher, O.; Guillet, F.; Bruneton, E.; Fiévet-Vincent, F.; Fiévet, F. *J. Mater. Sci.* **2000**, *35*, 3767.

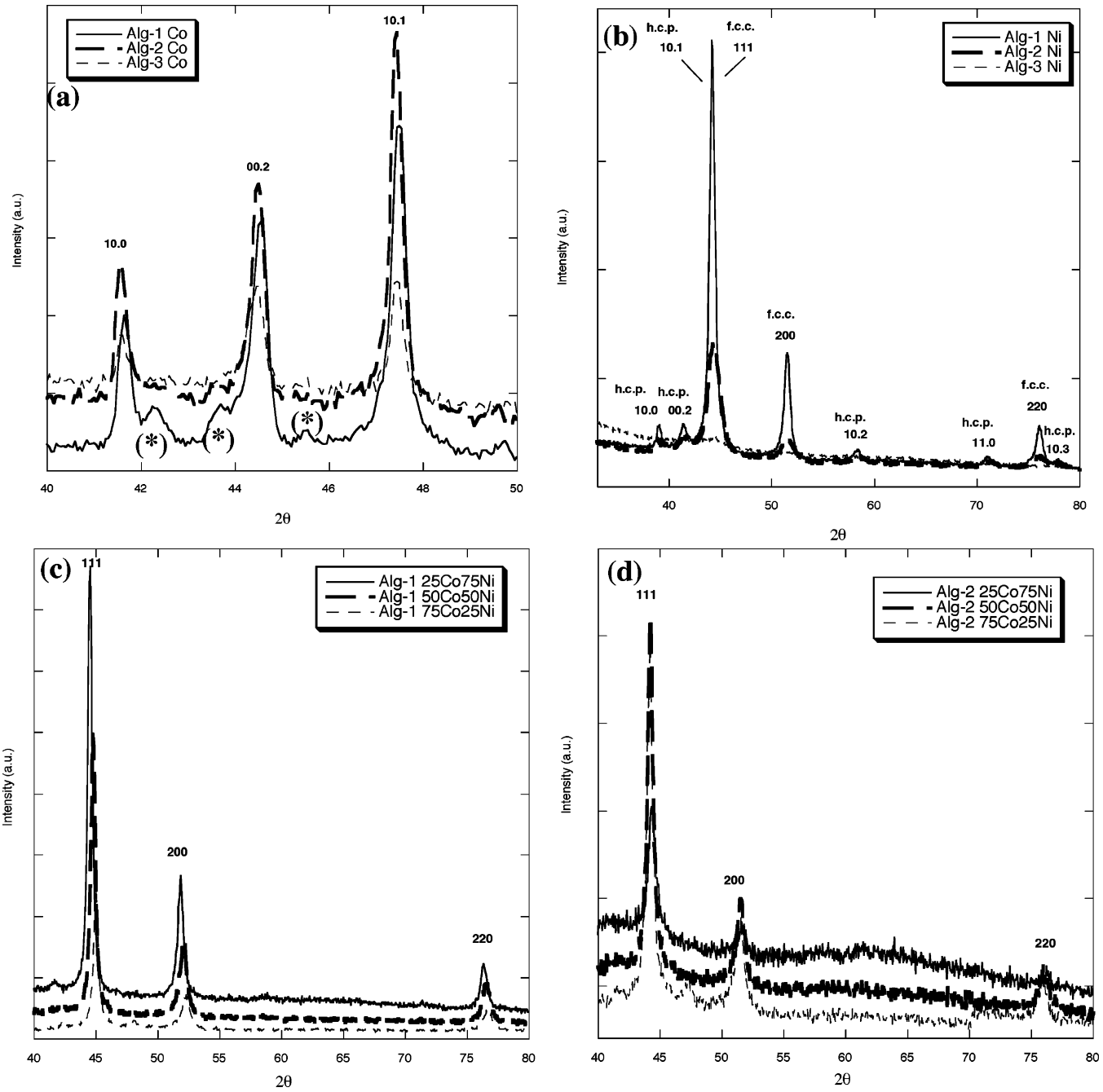

Figure 7. XRD patterns (after reduction at 350 °C) of (a) Co-based alginates, (b) Ni-based alginates, (c) Alg-1 CoNi solid solution, and (d) Alg-2 CoNi solid solution, recorded using Cu Kα radiation.

emu g^{-1}). According to the X-ray diffraction data, this can be related to the small dimensions of the particles whose high surface/volume ratio favors a higher degree of superficial oxidation and carbonaceous species formation.

The features of the zero-field-cooling/field-cooling (ZFC/FC) susceptibility curves of Alg-1 Ni reduced at 350 °C, reported in Figure 9, indicate a superparamagnetic behavior with a blocking temperature $T_B = 290$ K. Moreover, Alg-2 Ni and Alg-3 Ni are ferromagnetic at room temperature. The superparamagnetic behavior obtained with Alg-1 Ni sample is related to the hcp phase, exhibiting magneto-crystalline anisotropy, which is much less abundant in Alg-2 sample and lacking in Alg-3 Ni. Magneto-crystalline anisotropy arises from electron spin−orbit coupling. As the electron orbits are linked to the crystallographic structure, these coupling interactions induce a preferred orientation for spin alignment along well-defined crystallographic axes. For instance, in hexagonal crystals, the magneto-crystalline anisotropy energy is a function of the angle between the magnetization and the *c*-axis. Magneto-crystalline anisotropy is responsible for superparamagnetic behavior, and the blocking temperature T_B is known to be proportional to its energy. Moreover, in the ferromagnetic domain (below T_B), the existence of preferred magnetization directions influences the hysteresis width and the remanent magnetization. Thus Alg-1 Ni sample exhibits a high squareness ($S = M/M_s = 45$), and the coercitivity field obtained for this sample ($H_c = 434$ Oe) is higher than (i) Ni−gelatin prepared by radiolysis method ($H_c = 225$ Oe),[42] (ii) Ni−hexadecylamine nanorods ($H_c = 275$ Oe),[43] and (iii) close to Ni−TOPO (H_c

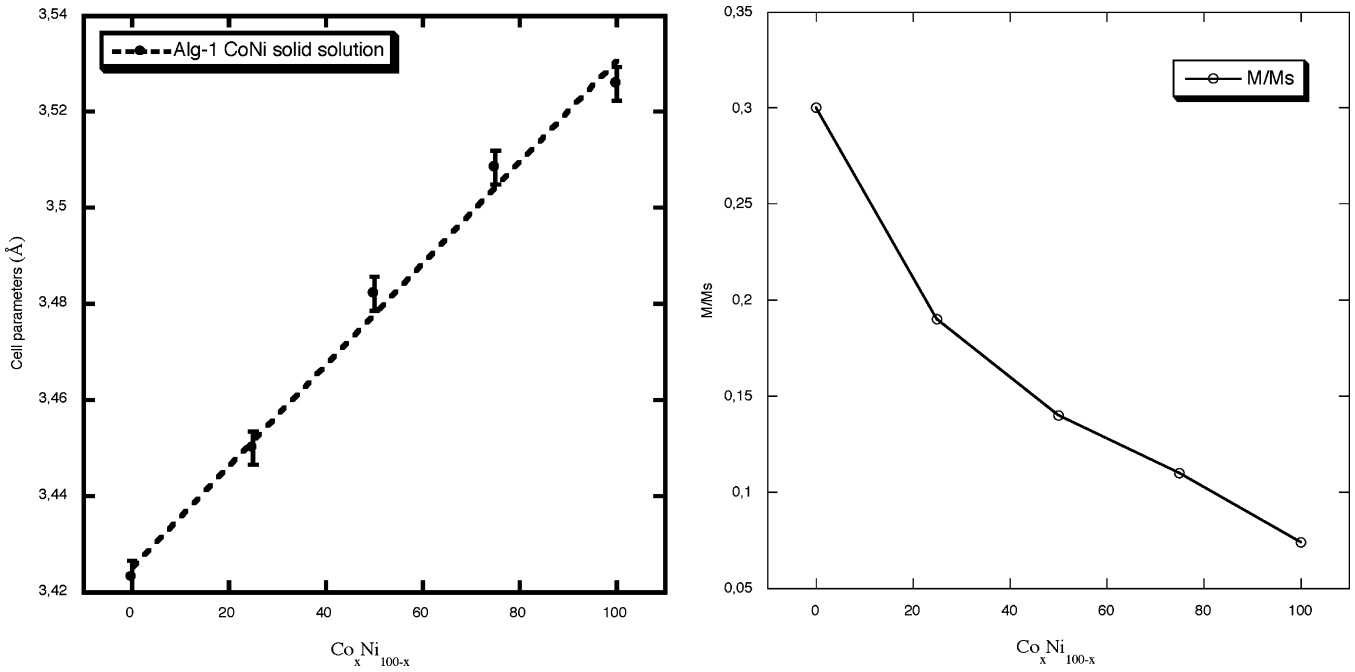

Figure 8. Correlation between solid solution composition and (a) fcc cell parameter and (b) coercitivity (H_C) and squareness (S) for Alg-1 CoNi samples.

Table 5. Magnetic Properties (Saturation Magnetization M_s, Coercitivity H_c, and Squareness S) of Alginate-Based NiCo at 2 K

sample	M_s (emu g^{-1})	H_c (Oe)	S
Alg-1 Ni	63	434	0.45
Alg-1 25Co75Ni	92	315	0.19
Alg-1 50Co50Ni	122	445	0.14
Alg-1 75Co25Ni	145	561	0.11
Alg-1 Co	148	574	0.07
Alg-2 Ni	54	355	0.25
Alg-2 50Co50Ni	106	530	0.26
Alg-2 Co	104	292	0.06
Alg-3 Ni	53	350	0.20
Alg-3 50Co50Ni	112	310	0.16
Alg-3 Co	105	291	0.05

$= 500$ Oe)[43] at 2 K (Table 5). It is worth noting that these results clearly indicate that these particles are formed of pure Ni phase and not of nickel carbide that usually present low M_s and H_c values,[44] in agreement with previous results.[15] All monometallic Co samples present surprising low squareness values for hcp phase,[45] which may also be attributed to the higher degree of superficial oxidation in agreement with X-ray diffraction data (Table 5 and Figure 9c). These values would be expected for isotropic structures. Figure 9d shows hysteresis loops of Alg-1 NiCo samples. For all alginates, saturation magnetization increases with Co concentration.

Finally, Figure 8b presents the variation of the magnetic properties with the chemical composition of $Co_xNi_{(100-x)}$ Alg-1 samples. Alg-1 Ni magnetic properties differ remarkably due to the presence of Ni hcp phase. This sample presents higher values of coercitivity and squareness than all Co and NiCo samples due to its magneto-crystalline anisotropy. For NiCo samples, the squareness value decreases with x, showing that Co is more easily oxidized than Ni. On the other hand, coercitivity values increase when x increases. The study of the influence of the chemical composition on the structure and the morphology of the NiCo particles confirms that, in the absence of hcp phase, isotropic growth is observed. In this case, Co coercitivity is higher than Ni one.

Conclusion

This study indicates that alginate is a suitable polymer to control the growth of monometallic and bimetallic metal nanoparticles. Metal cations act as cross-linkers for the formation of a gel network and are trapped within specific cavities where they are in close proximity. Upon reduction, these cavities can be pictured as confined media that limit the growth of the metal nanoparticles. If a mixture of cations is present, then the final stoechiometry of the resulting nanoalloys will depend on the relative affinity of the polymer for each of the trapped species. In addition, the intrinsic anisotropy of the cavity seems to affect the nature of the grown metallic phase, as shown here for Ni that adopts an unusual hcp structure.

In biomineralization processes, the ability of biological macromolecules to precisely control the growth of inorganic particles is indeed related to their specific chemical functionality and structure. In these processes, biological functions usually serve as nucleating centers and structure-directing agents for the mineral phase formation so that modification of their chemical functionality and/or spatial arrangement induces significant perturbation of the material morphology.[46] Whereas structure variability is limited for

(42) Kapoor, S.; Salunke, H. G.; Tripathi, A. K.; Kulshreshtha, S. K.; Mittal, J. P. *Mater. Res. Bull.* **2000**, *35*, 143.
(43) Cordente, N.; Respaud, M.; Senocq, F.; Casanove, M. J.; Amiens, C.; Chaudret, B. *Nano Lett.* **2001**, *1*, 565.
(44) Yue, L.; Sabiryanov, R.; Kirkpatrick, E. M.; Leslie-Pelecky, D. L. *Phys. Rev. B.* **2000**, *62*, 8969.
(45) Osuna, J.; de Caro, D.; Amiens, C.; Chaudret, B.; Snoeck, E.; Respaud, M.; Broto, J. M.; Fert, A. *J. Phys. Chem.* **1996**, *100*, 14571.
(46) *Biomineralization*; Baeuerlein, E., Ed; Wiley-VCH: Weinheim, 2004

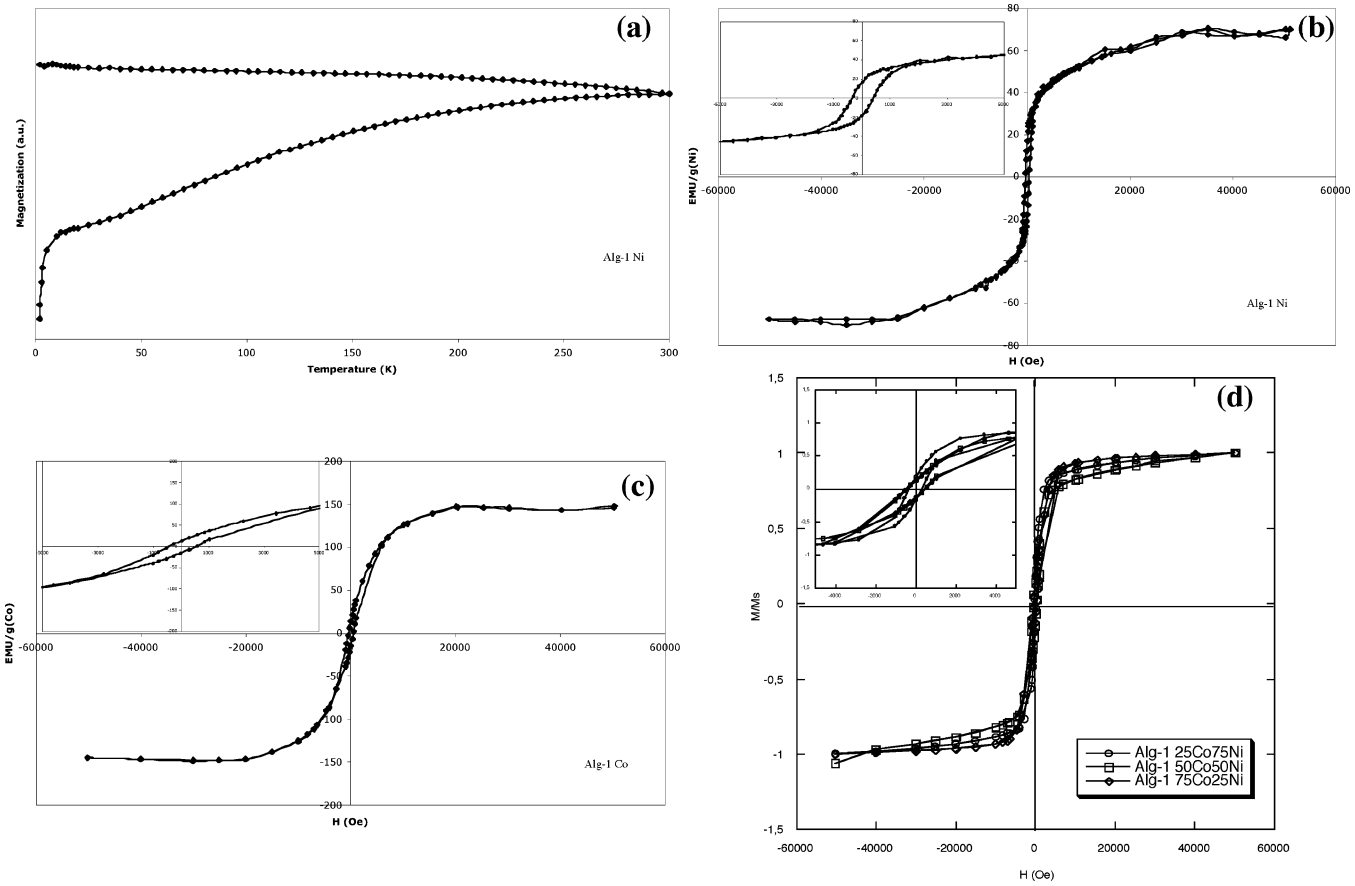

Figure 9. (a) ZFC/FC susceptibility curve of Alg-1 Ni (H = 500 Oe); (b) hysteresis loop for Alg-1 Ni at 2 K (insert: enlargement at low field); (c) hysteresis loop for Alg-1 Co at 2 K (insert: enlargement at low field); and (d) normalized magnetization (M/M_s) vs magnetic field for Alg-1 CoNi solid solutions at 2 K (insert: enlargement at low field).

proteins, polysaccharides can exhibit a wide range of different compositions depending not only on the organisms they are extracted from but also, for a given organism, on its environment.[17,47] The effect of such variability of biomacromolecules on their ability to control the growth of inorganic phase is demonstrated by our experiments showing that the variation in the M/G sugar ratio of the alginate copolymer has a strong influence on the crystallographic structure of the resulting metallic nanoparticles. This appears related to the strength of the gel network, which was shown to increase with the relative amount of guluronate groups[48] and hence to its capacity to confine the metal ions and control their aggregation during the reduction process, as shown for ligand-mediated growth of nanoparticles.[49]

Further studies are now in progress to extend this approach to other nanoparticle systems, such as oxides and chalcogenides. In parallel, in the context of the actual development of biopolymer-based materials,[50] the data presented here should be useful when considering the effect of natural macromolecule intrinsic variability on the properties of resulting biocomposites.

CM062580Q

(47) Hackney, J. M.; Kraemer, G. P.; Atalla, R. H.; Van der Hart, D. L.; Chapman, D. J. *Planta* **1994**, *192*, 1432.
(48) Smidsrod, O.; Haug, A. *Acta Chem. Scand.* **1972**, *26*, 79.
(49) Samia, A. C. S.; Hyzer, K.; Schlueter, J. A.; Quin, C. J.; Jiang, J. S.; Bader, S. D.; Lin, X. M. *J. Am. Chem. Soc.* **2005**, *127*, 4126.
(50) Coradin, T.; Allouche, J.; Boissière, M.; Livage, J. *Curr. Nanosci.* **2006**, *2*, 219.